Room temperature reduction of nitrogen oxide to nitrogen on Metal-Organic Frameworks

Marco Daturi[1]*, Vanessa Blasin-Aubé[1], Ji Wong Yoon[1,2], Philippe Bazin[1], Alexandre Vimont[1], Jong-San Chang[2,3]*, Young Kyu Hwang[2], You-Kyong Seo[2], Seunghun Jang[2], Hyunju Chang[2], Stefan Wuttke[1,4], M. Haneda[4], Patricia Horcajada[5], Christian Serre[5]

[1] *Normandie Univ., ENSICAEN, UNICAEN, CNRS, Laboratoire Catalyse et Spectrochimie, 14000 Caen, France.*

[2] *Catalysis Center for Molecular Engineering, Korea Research Institute of Chemical Technology (KRICT); Jang-dong 100, Yuseong, Daejeon 305-600, South Korea.*

[3] *Department of Chemistry, Sungkyunkwan University, Suwon 440-476, South Korea.*

[4] *Nagoya Inst. Technol., Grad. Sch. Engn., Dept. Frontier Mat., Showa Ku, Nagoya, Aichi 4668555, Japan*

[5] *Institut Lavoisier (UMR CNRS 8180), Université de Versailles Saint-Quentin-en-Yvelines, 45, avenue des Etats-Unis, 78035 Versailles, Université Paris Saclay, France. Present address : Ecole Normale Supérieure, Ecole Supérieure de Physique et de Chimie Industrielles de Paris, Paris Sciences Letter University, 75005 Paris, France*

Abstract

Air pollution is an epochal concern, particularly in urban areas, and is linked to combustion processes[1]. The emission of nitrogen oxides (NOx) constitutes a critical environmental problem, and it can affect severely human health[2,3,4]. At ambient temperature and pressure NOx decomposition is thermodynamically favoured; however, this process is kinetically inhibited, owing to a high activation energy[5,6]. To date, no reported catalysts have had the required properties to lower the activation energy of this process without the help of co-reacting agents and high temperatures[7,8,9]. Here, we show that NO conversion to molecular nitrogen can be achieved at room temperature in the presence of O_2 and H_2O vapour, and in the absence of any further reducing agent, using iron-based Metal-Organic Frameworks (MOFs). Further, we demonstrate that MOFs work similarly to enzymes, but are stable in environments unfriendly to living matter. These findings open large perspectives on the solution of stringent problems in chemistry, such as the removal of pollutants or the activation of highly stable molecules.

Introduction

The inorganic nitrogen cycle is the process by which nitrogen, in various chemical forms, is circulated by a continuous natural cycle[10]. Human activities in the modern industrial society have caused serious and diverse environmental problems, including interference with the nitrogen cycle both in aqueous and atmospheric environments. Although various methods have been adopted to reduce NOx selectively[11], some aspects of these technologies are still underdeveloped and further progress is still needed to overcome their drawbacks and cost limitations[12]. The daunting challenge to remove NOx in a sustainable way is to find a catalyst that is able to favour the decomposition reaction without being poisoned by oxygen[13], *i.e.* a catalyst ideally working at room temperature like enzymes, without the necessity of reducing agents. Denitrification in nature is based on an assortment of different enzymes that sequentially reduce nitrate to dinitrogen via nitrogen oxide intermediates, *e.g.*, nitrate reductase, nitrite reductase (NIR), nitric oxide reductase (NOR) and nitrous oxide reductase. These enzymes are mainly iron and copper based metalloenzymes[10,14]. However, enzymes are generally unstable out of aqueous solutions and therefore cannot be applied directly for the purification of polluted gases. Conversely, heterogeneous catalysts investigated to date are unable to imitate enzyme mechanisms, still requiring oxygen scavengers and/or high temperatures of reaction[11,15,16]. In fact, the active site environment in the metalloenzyme complexes is highly specific, as the result of million years of evolution. Catalysts that are intended to mimic enzyme mechanisms should therefore have a similar configuration[10,14,17].

The reduction of nitrites by heme-cd_1 is proposed to proceed via the binding of a nitrite to the reduced Fe^{II} centre with a concomitant dehydration/oxidation reaction to yield a putative 'oxidized' Fe^{III}-NO moiety. The active site of cNOR contains a heme/non-heme diiron centre, where the reduction of the diiron site weakens the oxo bridge and favours the coordination of two NO molecules. The NO molecules are coordinated in close enough proximity to destabilise these otherwise poorly reactive complexes and promotes the formation of a N-N bond[14]. With these examples in mind, we focused our attention on the mesoporous iron(III) trimesate MIL-100(Fe) (MIL stands for Materials from Institut Lavoisier) or $[Fe_3O(H_2O)_2F_{0.81}(OH)_{0.19}\{C_6H_3(CO_2)_3\}_2 \cdot nH_2O$ ($n \approx 14.5$)] as a possible candidate for the development of a new NOx removal (DeNOx) catalyst. MIL-100(Fe) is a hydrothermally stable MOF built up from oxo-centred trimers of iron(III) octahedra interconnected by 1,3,5-benzene tricarboxylate linkers giving rise to a mesoporous zeotype architecture (Fig. 1)[18].
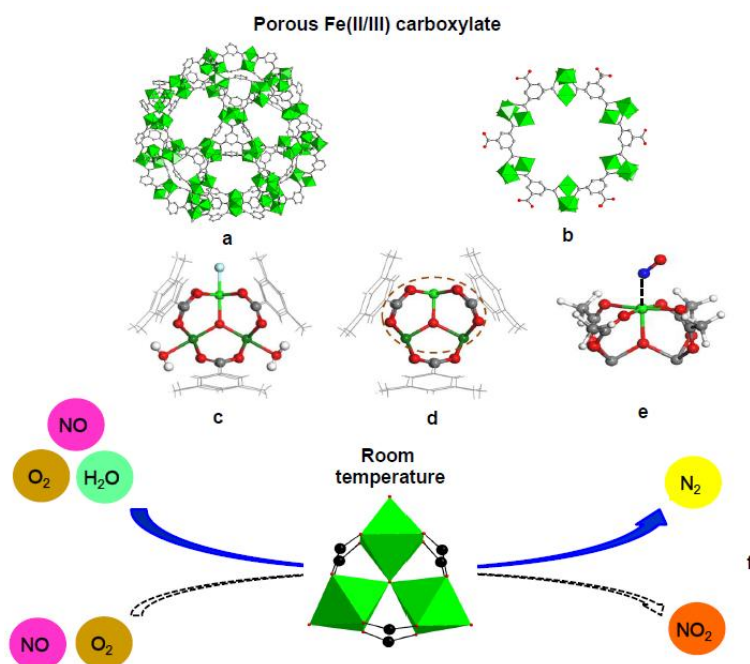
Figure 1: Schematic representation of the iron trimesate MIL-100(Fe) and the binding of NO over the iron metal sites. **a**, a mesoporous cage of MIL-100(Fe). **b**, A porous cage of MIL-100(Fe). **c**, View of one hydrated trimer of iron(III) octahedra. **d**, One dehydrated and defluorinated trimer of iron(II, III) octahedra. **e**, Coordination of one NO molecule over one Fe(II)/Fe(III) model cluster. **f**, Scheme of reaction behaviours on a mixed valent Fe^{II}/Fe^{III} trimer for the NO/O_2 and the NO/O_2/H_2O mixtures at room temperature.

We have previously shown that this solid exhibits accessible Fe^{II} and Fe^{III} coordinatively unsaturated metal sites upon thermal activation at 523 K[19]. Within each trimer of MIL-100(Fe), one Fe^{II} site is surrounded by at least one Fe^{III} site, imitating the unique environment observed in iron clusters of active NO reductive metalloenzymes, being this environment also indicated by preliminary density functional theory (DFT) calculations (see SI - Supplementary Information). This unusual property, which is specific to all Fe carboxylate-based MOFs built up from the same trimeric building unit[20], has been used to enhance the separation of hydrocarbons[19], and led to an improvement of the controlled release of NO as a biological gas[21].

Results and Discussion

MIL-100(Fe) was initially treated under argon for 5 h at 523 K to create Fe^{II}/Fe^{III} pairs in the trimer moieties (with a Fe^{II}/Fe^{III} ratio = *ca.* 0.3), as confirmed by *in-situ* IR spectroscopic analysis[22], UV-vis analysis and even XAS data. The DeNOx reaction at 300 K was tested using a wafer of casted MIL-100(Fe) powder to monitor the material in action spectroscopically under a gas reaction flow (gas hourly space velocity, GHSV = 5000 h^{-1})

typically containing 1000 ppm NO, 10% O_2, and 1% H_2O. For the sake of clarity, C-containing impurities such as CO_2, CO and hydrocarbons were carefully eliminated in the feed mixture. To our surprise, we found that up to 13% of the feed NO was catalytically and selectively converted to N_2 in the presence of O_2 and H_2O vapour, without any reducing agent. The resulting IR spectra of the catalyst under flow are presented in Fig. 2 a & b, where the adsorbed species evolving versus time are illustrated (Fig. 2c).
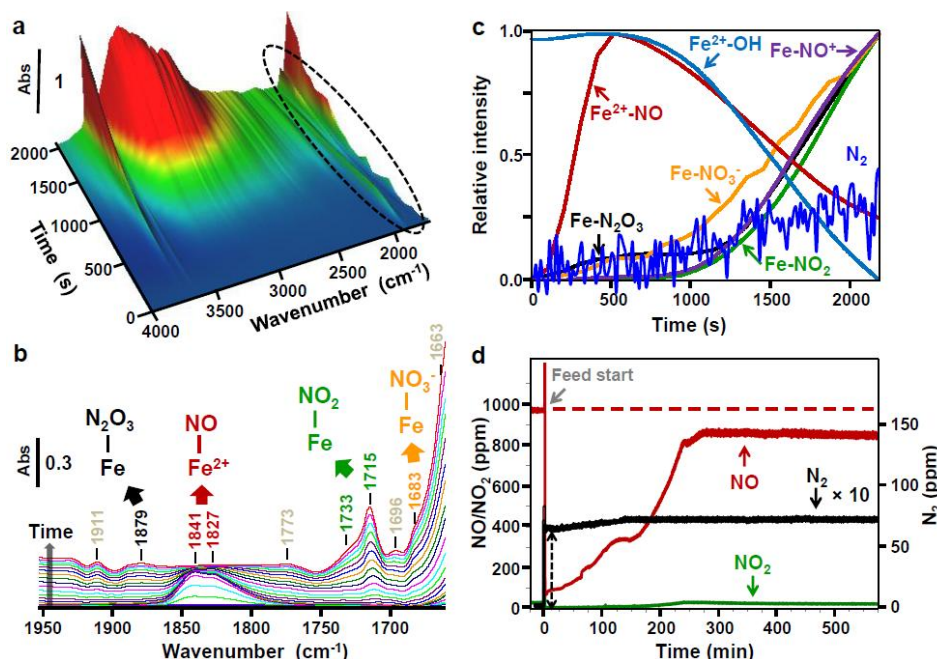

Figure 2: Surface and gas species during NO decomposition. **a**, 3D view of the transmission FTIR spectra in the vibrational MID-IR region of the MIL-100(Fe) sample activated at 523 K, then submitted to the reaction stream at 298 K. **b**, Waterfall of spectra (zoomed in the dotted region and subtracting the first spectrum in the series) collected every 105 s and during 2185 s, after about 33 min from t_0. They present only the modification of the material vibrations and of the adsorbed species. **c**, Intensity profiles versus time for the main species present on the surface of MIL-100(Fe) submitted to the reaction flow. The timeline is coherent with the spectra in Fig. 2b. **d**, Gas phase profiles for N-containing species during reaction, using Kr as an internal standard for the quantification of the species measured by a mass spectrometer.

Two phenomena appeared since the beginning: NO absorption by the sample and nitrogen production. While the first was protracted over a few hours (due to the large absorption capacity of the material[23]), the second rapidly reached a steady state (Fig. 2d). The selective formation of N_2 was confirmed by both the m/z = 28 signal observed by mass spectrometry and the absence of any other detectable N-containing species. Noteworthy, in a classical plug flow reactor NOx conversion was higher, reaching for example 34% at GHSV 15,000 h^{-1}, as detailed in SI; however, in order to get information on the gas phase and the catalyst behaviour simultaneously, we focus on the *operando* results.

The DeNOx reaction takes place only when Fe^{II} species are present, as indicated by the doublet IR peaks at 1841 and 1827 cm^{-1} (Fig. 2c), typical of Fe^{II}-nitrosyls[19]. In fact, when the sample was activated at 423 K, no Fe^{II} sites were detected via the adsorption of probe molecules and, consequently, no reactivity could be observed (Fig. 3b). However, upon further activation of this sample at 523 K, Fe^{II} species were clearly evidenced by IR spectroscopy, and the NO conversion activity was observed, as previously shown in Figs. 2. Thus, the catalytic activity of MIL-100(Fe) is unambiguously related to the presence of Fe^{II} sites. Furthermore, the presence of oxygen and water in the gas flow is essential for the DeNOx reaction (Fig. 3 and SI), which could allow us to gain an understanding into the mechanism operating here.
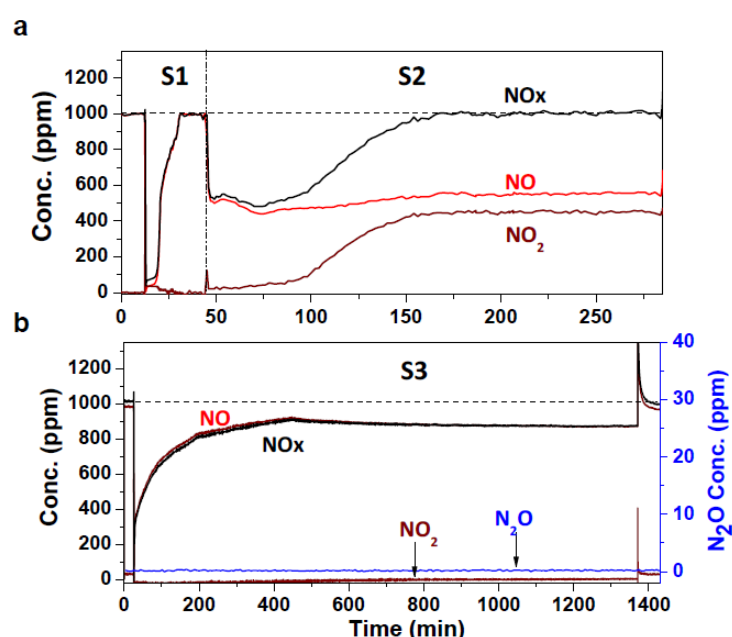

Figure 3: Effect of the gas composition on the catalytic reaction. Main species profiles in the gas phase after contact with partially reduced MIL-100(Fe) sample at 298 K. **a** Sequential gas feeding with 1000 ppm NO (S1) followed by 1000 ppm NO with 10% O_2 (S2), and **b**, 1000 ppm NO, 10% O_2 and 1% H_2O vapour (S3). The profiles of NO and NO_2 were measured by NOx analyser, while the profile of N_2O was collected by an IR gas analyser.

Obviously, detailed comprehension of the mechanism of NO reduction into N_2 on MIL-100(Fe) (beyond the scope of the present study) would require further extensive and dedicated investigations. The reactions involved in DeNOx are extremely complex, and the proposed mechanisms are still under debate[11], even after decades of investigation. Nevertheless, some of our spectroscopic evidences highlight the formation of adsorbed species (see SI and Extended Data Figure 9) which can be related to those proposed for the reduction of nitrites by the heme cd_1-containing NIR[10] and for the NOR[14] in fungal and bacterial enzymes. The

latter, in particular, have the active structure that consists of a binuclear oxo-bridged heme/non-heme iron active site, in which the μ-oxo-bridged Fe-O-Fe moiety has a Fe-Fe distance of 3.5 Å and a (Fe-O-Fe) angle of 145° [14]. In MIL-100(Fe), the distance between the two iron sites in the trimers is close to 3.4 Å with a (Fe-O-Fe) angle of 120°. These structural similarities allow us to postulate a common mechanism between enzymatic catalysis and NO removal by MOFs, where the organic-inorganic hybrid structure of MIL-100(Fe) would behave as a solid homologue of the organometallic cluster at the core of the NOR. This would explain the slow measured reactivity, which is a typical feature of enzymatic driven mechanisms[10]. Similar conclusions have been proposed recently to explain selective catalytic reduction of NOx with NH_3 on Cu-exchanged SSZ-13 zeolites [24] as well as oxidation phenomena of ethane with N_2O, observed on the microporous iron hydroxyterephthalate MOF-74 or CPO-27(Fe)[25]. However, in the latter case the presence of monomeric Fe^{II} sites in the CPO-27 structure makes this material likely unsuitable for DeNOx reaction, besides the fact that this material also suffers from instability towards water and oxygen.

If the hypothesised mechanism requires the presence of neighbouring Fe^{II}/Fe^{III} unsaturated sites, other iron carboxylate analogues should also be active towards NO conversion at room temperature. Significantly, the microporous iron 3,3',5,5'-azobenzenetetracarboxylate MIL-127(Fe) solid, that exhibits the same constitutive iron trimers, showed a similar reactivity (see SI). Conversely, the iron 1,4,5,8-naphthalentetracarboxylate MIL-102(Fe) solid based on the same trimers but exhibiting very narrow pores (< 4 Å), and the flexible microporous iron terephthalate MIL-53(Fe) solid containing a different building unit with no accessible metal sites (see SI), were both inactive for the DeNOx reaction. This indicates that the combination of iron trimers and pore accessibility is a prerequisite for NO transformation under ambient conditions.

Conclusions and Outlook

Our strategy therefore proposes the use of stable highly porous iron carboxylates bearing both accessible Fe^{II} and Fe^{III} sites as catalytic materials to decompose NOx at room temperature without any reducing agent. This strategy can potentially lead to major breakthroughs in the particular domain of NOx removal and represents a concrete progress in the use of MOFs as a new class of heterogeneous catalysts. Probably they will never been able to stand the extreme conditions of an automotive exhaust, but they could be used for NOx abatement in confined polluted ambient, such as undergrounds parking, tunnels, factories, etc. But the most important is our proof of concept: conceptually, we are on the way to demonstrate that MOFs

are a class of materials that bridge the gap between homogeneous (enzymatic) and heterogeneous (solid) catalysis by mimicking organometallic compounds. The iron-based MOFs proposed in this work are stable in the presence of moisture, relatively inexpensive to be industrially synthesised[26,27], easily recyclable, and bio-compatible[28], and are therefore likely to pave the way for new generations of highly efficient and sustainable catalysts[29]. In perspective, MOFs-based catalysts can face different challenging problems such as VOC abatement, light alkanes or CO_2 activation, upon an appropriate rational tailoring.

References

[1] Buchholz, S. *et al.* Air pollution characteristics associated with mesoscale atmospheric patterns in northwest continental Europe. *Atmos. Environ.* **44**, 5183-5190 (2010).

[2] Samoli, E. *et al.* Short-term effects of nitrogen dioxide on mortality: an analysis within the APHEA project. *Eur. Respir. J.* **27**, 1129-1137 (2006).

[3] Peters, A. *et al.* Air pollution and incidence of cardiac arrhythmia. *Epidemiology* **11**, 11-17 (2000).

[4] Arden Pope, C. III *et al.* Cardiovascular mortality and long-term exposure to particulate air pollution: Epidemiological evidence of general pathophysiological pathways of disease. *Circulation* **109**, 71-77 (2004).

[5] Fritz, A. & Pitchon, V. The current state of research on automotive lean NOx catalysis. *Appl. Catal. B: Environmental* **13**, 1-25 (1997).

[6] Gomez-Garcıa, M.A., Pitchon, V. & Kiennemann, A. Pollution by nitrogen oxides: an approach to NO(x) abatement by using sorbing catalytic materials. *Environment International* **31**, 445-467 (2005).

[7] Hamada, H., Kintaichi, Y., Sasaki, M. & Ito, T. Sulfate-promoted metal oxide catalysts for the selective reduction of nitrogen monoxide by propane in oxygen-rich atmosphere. *Chem. Lett.* **20**, 2179-2182 (1991).

[8] Haneda, M., Kintaichi, Y., Bion, N. & Hamada, H. Alkali metal-doped cobalt oxide catalysts for NO decomposition. *Appl. Catal. B: Environmental* **46**, 473-482 (2003).

[9] Neyertz, C., Volpe, M.A. & Gigola, C. Palladium-vanadium interaction in binary supported catalysts. *Catal. Today* **57**, 255-260 (2000).

[10] Averill, B.A. Dissimilatory nitrite and nitric oxide reductases. *Chem. Rev.* **96**, 2951-2964 (1996).

[11] Granger, P. & Parvulescu, V.I. Catalytic NOx abatement systems for mobile sources : From three-way to lean burn after-treatment technologies. *Chem. Rev.* **111**, 3155-3207 (2011).

[12] Klingstedt, F., Arve, K., Eränen, K. & Murzin, D.Y. Toward improved catalytic low-temperature NOx removal in diesel-powered vehicles. *Acc. Chem. Res.* **39**, 273-282 (2006).

[13] Amirnazmi, A., Benson, J.E., & Boudart, M. Oxygen inhibition in the decomposition of NO on metal oxides and platinum. *J. Catal.* **30**, 55-65 (1973).

[14] Wasser, I.M. *et al.* Nitric oxide in biological denitrification: Fe/Cu metalloenzyme and metal complex NOx redox chemistry. *Chem. Rev.* **102**, 1201-1234 (2002).

[15] Iwamoto, M. & Hamada, M. Removal of nitrogen monoxide from exhaust gases through novel catalytic processes. *Catal. Today* **10**, 57-71 (1991).

[16] Shelef, M. Selective Catalytic Reduction of NO, with N-Free Reductants. *Chem. Rev.* **95**, 209-225 (1995).

[17] Ford, P.C. & Lorkovic, I.M. Mechanistic Aspects of the Reactions of Nitric Oxide with Transition-Metal Complexes. *Chem. Rev.* **102**, 993-1017 (2002).

[18] Horcajada, P. *et al.* Synthesis and catalytic properties of MIL-100(Fe), an iron(III) carboxylate with large pores. *Chem. Commun.* 2820-2822 (2007).

[19] Wuttke, S. *et al.* Discovering the active sites for C_3 separation in MIL-100(Fe) by using operando IR spectroscopy. *Chem. Eur. J.* **18**, 11959-11967 (2012).

[20] Devic, T. & Serre, C. High valence 3p and transition metal based MOFs. *Chem. Soc. Rev.* **43**, 6097-6115 (2014).

[21] McKinlay, A.C. *et al.* Nitric oxide adsorption and delivery in flexible MIL-88(Fe) metal-organic frameworks. *Chem. Mater.* **25**, 1592-1599 (2013).

[22] Leclerc, H. *et al.* Infrared study of the influence of reducible iron(III) metal sites on the adsorption of CO, CO_2, propane, propene and propyne in the mesoporous metal-organic framework MIL-100. *Phys. Chem. Chem. Phys.* **13**, 11748-11756 (2011).

[23] Eubank, J.F. *et al.* Porous, rigid metal(III)-carboxylate metal-organic frameworks for the delivery of nitric oxide. *APL Mater.* **2**, 124112 (2014).

[24] Kwak, J.H. *et al.* Common intermediate for N_2 formation in enzymes and zeolites: Side-on Cu-nitrosyl complexes. *Angew. Chem., Int. Ed.* **52**, 9985-9989 (2013).

[25] Xiao, D.J. *et al.* Oxidation of ethane to ethanol by N_2O in a metal–organic framework with coordinatively unsaturated iron(II) sites. *Nature Chem.* **6**, 590-595 (2014).

[26] Seo, Y.-K *et al.* Large scale fluorine-free synthesis of hierarchically porous iron(III) trimesate MIL-100(Fe) with a zeolite MTN topology. *Micropor. Mesopor. Mater.* **157**, 137-145 (2012).

[27] Gaab, M., Trukhan, N., Maurer, S., Gummaraju, R., Muller, U. The progression of Al-based metal-organic frameworks - From academic research to industrial production and applications. *Micropor. Mesopor. Mater.* **157**, 131-136 (2012).

[28] Horcajada, P. *et al.* Porous metal-organic-framework nanoscale carriers as a potential platform for drug delivery and imaging. *Nature Mater.* **9**, 172-178 (2010).

[29] Gascon, J., Corma, A., Kapteijn, F., Llabrés i Xamena, F.X. Metal Organic Framework Catalysis: Quo vadis? *ACS Catal.* **4**, 361-378 (2014).

Methods

Material synthesis. MIL-100(Fe), MIL-127(Fe), MIL-102(Fe) and MIL-53(Fe) were hydro/solvothermally prepared as described elsewhere[18,30,31] (see SI for further details).

In situ **IR characterization of MIL-100(Fe).** Self supported samples were analysed in a quartz cell, using adapted probe molecules (see SI for further details and reference[32]).

Operando **IR investigation of MIL-100(Fe).** The IR *operando* system used for this study is constituted by a custom-made flow setup, a specifically developed reactor-cell and a set of gas analysers, as specified in SI and reference[19]. It allows a thorough time-resolved analysis of solid-gas heterogeneous catalytic reactions. In particular, the possibility to follow the IR surface spectra versus time, in parallel with the gas composition (sharing gas analysis via the simultaneous use of an IR gas analyser, a chemiluminescence and a mass spectrometer) allows investigating the reaction pathway from a qualitative and quantitative point of view.

The sample was firstly activated at 523 K or 423 K (according to the purposes of the experiment, as discussed in the paper) under a flow of argon for 5 hours, to eliminate traces of impurities and adsorbed water. For the sake of clarity, we carefully excluded C-containing impurities such as CO_2, CO and hydrocarbons in a feed mixture, even if habitually present in a combustion exhaust. Then a flow containing 1000 ppm NO, 10% O_2, 1% H_2O in Ar as the vector gas was introduced into the cell heated at about 300 K (space hourly velocity varying between 5000 and 80000 h^{-1}).

MIL-100(Fe) cluster model DFT calculations for NO binding. The cluster model calculations were carried out based on first principles density functional theory (DFT) calculations, implemented in $DMol^3$ and Vienna Ab initio Simulation Package (VASP). More detailed procedures and results on the calculations are described in the SI.

---

[30] Serre, C. et al. Utilisation d'un solide hybride cristallin poreux comme catalyseur de réduction d'oxydes d'azote et dispositifs, 106660/FR patent filed 28/05/2009 ; PCT/ FR2010/000402 (28/05/2010)

[31] Horcajada, P. et al. *J. Am. Chem. Soc*. **130**, 6774-6780 (2008).

[32] Vimont, A., Thibault-Starzyk, F., Daturi, M. Analysing and understanding the active site by IR spectroscopy, *Chem. Soc. Rev.* **39**, 4928-4950 (2010).

Author Contributions M.D. designed the study, analysed data and wrote the paper. V.B.-A. and J.W.Y. collected data and treated them. P.B. supervised the *operando* investigation and adapted the system to the study specificities. A.V. performed the *in situ* investigation. J.-S.C. equally contributed to the design of this work and to the paper writing. Y.K.H. and Y.-K.S. performed the synthesis of materials and their characterisation. S.J and H.C. performed molecular simulation. C.S. contributed to the study and the paper writing. P.H. performed the synthesis of the materials and their characterisation. S.W. also participated to characterisations. All authors discussed the results and commented on the manuscript.

Supplementary Information

Structure and synthesis of MOF solids
MIL-100(Fe)

MIL-100(Fe) is a trivalent metal carboxylate MOF with the chemical composition $Fe_3O(H_2O)_2F_{0.81}(OH)_{0.19}\cdot(C_6H_5(CO_2)_3)_2\cdot nH_2O$ (n ~ 14.5). As illustrated in Fig. 1 and Extended Data Figs. 2 and 3, MIL-100(Fe) consists of iron trimers (the secondary building unit) and 1,3,5-benzene tricarboxylic (the organic linker), which construct the so-called supertetrahedra[18]. The resulting structure exhibits several interesting features: a mesoporous zeotype architecture (Extended Data Fig. 2c) with a MTN (MTN = zeolite socony mobil-thirty-nine) topology[33], a huge unit cell volume ($V_{u.c.}$ = 388 000 $Å^3$), two mesoporous cages (cage diameters: 25 and 29 Å – highlighted in Extended Data Fig. 2c as green (25 Å) and red (29 Å) cages – that are accessible through micropourous windows (5 and 9 Å), a high porosity (BET surface area >2000 m^2 g^{-1} and pore volume ~ 1.2 $cm^3.g^{-1}$) and a temperature stability under high vacuum until 523 K[18]. Moreover, it was already demonstrated for MIL-100(Cr) and MIL-100(Fe) by using *in situ* IR spectroscopy, that each metal octahedron possesses one terminal group, where H_2O, OH^- or F^- is adsorbed after the synthesis and it can transform in a undercoordinated site after temperature activation[22,34]. In the case of MIL-100(Fe), there is the possibility of the generation of iron CUS with mixed valence Fe^{II}/Fe^{III} by temperature treatment[35]. Despite the creation of Fe^{II} and Fe^{III} CUS, the overall structure of MIL-100(Fe) does not change[19,35].

MIL-100(Fe) was hydrothermally synthesized in presence of HF as previously reported[18]. Activation of MIL-100(Fe) consisted in the suspension of 2.5 g of the as-synthesized solid in 350 mL of water at 70°C for 3 h and then in 200 mL ethanol at 60°C for 3 h. Further activation was carried out by redispersing the solid in 100 mL of a 38 mM aqueous NH_4F solution at 70°C for 3 h, subsequently recovering the solid by filtration and repeating a water washing (350 mL at room temperature for 3 h) to remove the remaining NH_4F.

MIL-127(Fe) of *Soc*-MOF(Fe)

MIL-127(Fe), isostructural to *soc*-MOF(In) reported by Eddaoudi *et al.*[36], is built from iron(III) octahedra trimers linked by the 3,3',5,5'-azobenwenetetracarboxylic acid linkers, leading to the chemical formula $Fe_3OF(H_2O)_3(C_{16}N_2O_8H_6)_{1.5}.nH_2O$. Each trimer unit is linked by six separate ditopic organic linkers to build up a 3D cubic structure. In each octahedron, the apical position is occupied by a terminal water molecule. Each trimer unit is linked by six separate organic linkers to produce a cubic 3D structure with the *soc* topology (Extended Data Fig. 3b).[37] Each iron atom is trivalent, yielding an overall cationic framework (+1 per formula unit) that is balanced here by fluorine ions. This solid exhibits an important porosity ($S_{BET} \sim$ 1400 $m^2 \cdot g^{-1}$, $V_p \sim 0.7$ $cm^3 \cdot g^{-1}$) with two types of pores: i) an accessible 1D channels system (~ 5-7 Å), and cages of ~ 10 Å accessible through windows of ~ 3 Å, allowing only the adsorption of small molecules such as H_2O or H_2.

MIL-127(Fe) was solvothermally synthesized as previously reported[38]. The resulting product was filtered, washed with dimethylformamide and then heated at 200°C under primary vacuum for 15 h.

MIL-102(Fe)

MIL-102 is also a trivalent metal carboxylate MOF based on iron(III) octahedra trimers connected, in this case, by 1,4,5,8-naphthalentetracarboxylate, leading to the chemical formula $Fe_3O(OH)(H_2O)_2[C_{10}H_2-(CO_2)_4]_{1.5}.nH_2O$.

Iron(III) octahedra trimers link through the naphthalentetracarboxylate anions, creating a hexagonal three-dimensional framework ($V_{u.c.} \sim 1330$ $Å^3$; Extended Data Fig. 3c). Each iron atom exhibits an corner-sharing octahedrally coordinated environment with four oxygen atoms from the bidentate carboxylates, one $\hat{t}3$-oxo atom, and one terminal site. The latter site can be occupied by a terminal water molecule and/or an anion (typically -OH), leading to the formation of a trimeric iron subunit. Along [001], each trimer is connected to its equivalent by the bridging carboxylate functions of the organic moiety. A special kind of nanotube which shares the central C-C bond of the naphthalene groups is formed. The hexagonal arrangement of such nanotubes creates 1D pore channels of ~3-4 Å along the *c*-axis, where six free water molecules are located. Terminal water molecules or hydroxy anions point toward the center of the tunnels.

MIL-102(Fe) was hydrothermally synthesized as previously reported[30]. The resulting product was purified by suspending 2.5 g of the as-synthesized solid in 350 mL of ethanol at room temperature for 3 h. This procedure was repeated until the complete removal of the free ligand, as confirmed by IR.

MIL-53(Fe)

MIL-53(Fe) is built up from chains of *trans* corner-sharing of iron(III) octahedra (Extended Data Fig. 3d) joined together in the two other directions via terephthalate anions[39], creating a three-dimensional structure with a diamond-shape microporous 1D pore system (Extended Data Fig. 3d). MIL-53 exhibits a flexible structure[40,41,42], able to reversibly adapt its pore size in presence of different *stimuli* (temperature, guest adsorption, pressure), from a close form ($V_{u.c.} \sim$ 900-1000 Å^3 Ø $\sim$ 4 Å) to an open form ($V_{u.c.} \sim$ 1400-500 Å^3; Ø $\sim$ 8.5 Å) with a variation of their cell volume (up to 40%) without any bond breaking.[43]

MIL-53(Fe) was solvothermally synthesized as previously reported[30]. The resulting product was purified by suspending 2.5 g of the as-synthesized solid in 350 mL of ethanol at room temperature for 3 h. This procedure was repeated until the complete removal of the free ligand, as confirmed by IR.

DFT calculations

To analyse the consequences of the oxidation state of the iron sites over the NO binding, cluster model calculations of MIL-100(Fe) based on first principles density functional theory (DFT) calculations, were first carried out.

Firstly, we construct a cluster model including a symmetric Fe trimer from the reported MIL-100(Fe) structure[18], as shown in Extended Data Fig. 4(a). This large cluster for hydrated model consists of Fe_3O $(F)(H_2O)_2$ $[(C_6H_3)(CO_2)(Me)_2]_6$ units, where two ending (CO_2)'s of trimesate are replaced by methyl group (Me)s. Then the atomic structure of the large cluster was optimized to give the lowest total energy as keeping trimesate structure using Dmol^3 code[44,45]. For hydrated large cluster calculations, we can confirm two different Fe oxidation states, Fe(III) facing H_2O and Fe(II) facing F from the molecular orbital analysis. In order to investigate the electronic structures of Fe in a more detailed manner, we built a smaller cluster including "one" Fe atom with F, as shown in Extended Data Fig. 4(b), from the optimized atomic structure of the large cluster. This small cluster consists of $(FeO)(F)((CO_2)Me)_4C_2$ units, where $[(C_6H_3)(CO_2)_3]$ was replaced by $((CO_2)Me)$ and the other two Fe atoms of the Fe trimer were replaced by carbon atoms keeping the atomic and electronic structure of the large cluster. For the small Fe cluster calculations, we used the Vienna Ab initio Simulation Package (VASP)[46]. Starting from a fluorinated small cluster, Fe(II) was obtained by removing F atom, whereas Fe(III) was obtained by removing F^- ion. We found that the high spin states of Fe(II) and Fe(III) have the lowest total energies, as spin quintet (S=4) and spin sextet (S=5), respectively. For the investigation of the NO binding characters, the binding energies and charge transfer amount of NO molecule to Fe(II) and Fe(III) were calculated, as listed in the table Extended Data Fig. 4(c). NO molecule binds to Fe ions with an angle of about 120-140°. NO molecule is more strongly bound to Fe(II) than Fe(III) with an higher binding energy and a shorter distance. The Bader charge[47] values were used to calculate the charge transfer of the NO molecule. The charge transfer of NO to Fe(II) is bigger than to Fe(III), and the electron transfer directions are opposite. NO molecule tends to attract electrons from Fe(II), whereas it tends to lose electrons to Fe(III). When NO molecule is bound to Fe(II) strongly, the distance between N and O is getting longer than its molecular distance for the free molecule, therefore NO intramolecular bonding could be weakened when the species is bound to Fe(II). That can explain why Fe(II) sites are more active in NO

dissociation.

In our DFT cluster calculations, we used two different DFT codes, Dmol^3 and VASP codes. DMol^3 was used to determine the atomic structures and oxidation states of Fe ions with the big cluster model. VASP code was used for NO binding state with small cluster models, for more accurate description of spin states of Fe, since VASP is known to give a good agreement with experiments for magnetism of Fe ion. In both calculations, the spin-unrestricted DFT cluster calculations were carried out with the Perdew−Burke−Ernzerhof (PBE) functional. For Dmol^3 calculations, the numerical basis set of DNP and DFT semicore pseudopotentials (DSPPs) for Fe were employed and van der Waals interactions are included within Tkatchenko–Scheffler (TS)[48] scheme, as implanted in Dmol^3. In the VASP code, periodic plane-wave basis sets are used with frozen-core projector augmented wave (PWA) pseudopotentials[49]. For Fe atoms, GGA+U was employed with U = 2.5 eV. In VASP calculations, van der Waals interactions are also included with Grimme scheme[50].

Reaction tests in a catalytic reactor

A sample of MIL-100 (Fe) of about 1.5 g was put in a tubular reactor connected to a system for introduction and analysis of gas phases (by gas chromatography and mass spectrometry). The sample was pretreated by passing a helium stream (100 mL/min) over it for 6h at 250°C. The experiment was then conducted at 30°C, under a mixture of 1000 ppm of NO and He as carrier gas, adding or not 10% of oxygen and 1% of water. The total flow was set to obtain a space velocity of 15000 h^{-1}.

When NO only is sent to the reactor, only absorption phenomena are observed. In the presence of oxygen and absence of water, 82% of NO is converted into NO_2 after contact with MIL-100(Fe) powder. Feeding the reactor with the full gas mixture (NO + O_2 + H_2O in He) provides a steady conversion of NOx into N_2, reaching an efficiency of 34%.

In situ **IR characterization**

Samples were pressed (~10^2 MPa) into self-supported disks (2 cm^2 area, 7–10 mg cm^{-2}) and placed in a quartz cell equipped with KBr windows. A movable quartz sample holder permits one to adjust the pellet in the infrared beam for spectra recording and to displace it into a furnace at the top of the cell for thermal treatment. The cell was connected to a vacuum line for evacuation ($P_{residual} \cong 10^{-4}$ Pa) and for the introduction of gases into the infrared cell. Spectra were recorded at room temperature, except in the case of CO adsorption experiment where the pellet was maintained at 100 K by cooling the sample holder with liquid nitrogen after quenching the sample from the thermal treatment. The addition of well known doses of gases in the cell was possible via a calibrated volume connected to a pressure gauge for the control of the gas pressure. A Nicolet Nexus spectrometer equipped with a Mercury Cadmium Telluride (MCT) cryodetector and an extended KBr beam splitter was used for the acquisition of spectra recorded at room temperature in the 600–5500 cm^{-1} range. IR spectra are absorbance spectra and the notation used is a.u. for absorbance units. The resolution of the spectra was 4 cm^{-1}, and 256 scans were accumulated for each spectrum. A self-supported MIL-100(Fe) solid strongly absorbs the IR light between 1300 and 1650 cm^{-1} (region of the carboxylates stretching vibrations).

Operando **IR characterisation**

The IR *operando* system, which was used for this study, is composed of four main parts: the infrared spectrometer, the IR reactor-cell, the gas flow set-up and the exhaust gas analysers. The cell was connected to the *operando* gas-system including mass flow controllers for the introduction of gases into the lines. Two gas mixtures can be prepared and sent independently to the reactor cell. The system allows investigating the exhaust gases (reactive and/or reaction products) simultaneously by a Quadrupole Mass Spectrometer (Pfeiffer Omnistar GSD 301), an IR gas micro-cell of 0.088 cm^3 volume and a Thermo Electron model 10A rack-mounted Chemiluminescent NO-NOx gas analyser at the same time. This is a very important option to follow qualitatively and quantitatively the molecular composition of the gas: some of the molecules can be measured only by a single instrument, while the molecules detected by multiple analysers permit to verify the coherence among the experimental data. IR spectra (64 scans per spectrum) are collected with a Thermo Scientific Nicolet 6700 spectrometer, equipped with a MCT detector. More details can be found in the following references[51-53]. The IR reactor-cell used in this study is a so-called "Sandwich" *operando* cell developed by the LCS scientists and engineers, and described in details elsewhere[19]. This apparatus works in the domain of temperature 298-873 K. The sample is placed in the toroidal sample holder (in the centre of the cylindrical body) in the form of a self-supported wafer of 8-9 mg cm^{-2}. The required tightness of the cell can be obtained by using Kalrez O-rings between the terminal KBr windows and the extremities of the cell. The rest of the space is filled by KBr windows, which limit the reactor volume to 0.42 cm^3. The experiment was carried out at atmospheric pressure; gases are introduced onto the sample by a 1/8" OD pipe and collected on the opposite side of the sample holder.

Detailed analysis of the time-resolved gas composition and infrared spectra of the sample

The DeNOx reaction has been tested several times, both in the *operando* setup and in a classical plug flow reactor, to ensure a correct repeatability[30]. Note that a casted wafer presents a lower catalytic efficiency respect to the corresponding powder, as pointed out in[54]. Nevertheless, it provides spectroscopic evidences useful for the comprehension of the chemical process. Leaving the catalyst under stream up to 3 days does not change the NO conversion, nor the nitrogen yield, within the experimental error, as shown in Extended Data Fig. 5, for example. This is a very important point, since it demonstrates the catalytic nature of the reaction. In fact, the experimental data show that a stable conversion of NOx is obtained over more than 3000 min. Therefore, if the conversion is of at least 13% in a gas flow (25 mL/min) containing 1000 ppm NO, i.e. corresponding to a NOx conversion above 130 ppm over the entire period, more than 1350 μmol of NOx are converted per gram of catalyst, well above the maximum amount of 850 μmol/g of Fe^{2+} sites measured after reducing MIL-100(Fe)[22]. This rule out the possibility of a molecular reaction. Thus, when the gas feed is in contact with the sample activated at 523 K under Ar, a catalytic transformation of NO into dinitrogen can be observed (Figure 2d), concurrently with the formation of Fe^{II} dinitrosyls (Figure 2b). This conversion (for a casted sample: 13% at the gas hourly space velocity, GHSV = 5000 h^{-1}; 8% for a GHSV of 15,000 h^{-1}; 4.5% for a GHSV = 80,000 h^{-1}) is selective, as evidenced by both the signal m/z = 28 in mass spectrometry and the absence of

any other detectable N-containing species, such as N_2O or ammonia, easily detectable by IR. On the contrary, if the sample is activated, for example, at 423 K no Fe^{II} sites are detectable on the surface via the adsorption of probe molecules and no reactivity can be observed (Extended Data Figure 1), except for a partial NO to NO_2 oxidation. If the same sample is further activated at higher temperature, Fe^{2+} species are clearly seen and the NO dissociation activity starts, as previously shown in Figure 2. Therefore the catalytic activity is linked to the presence of Fe^{2+} sites, promoted by the treatment at higher temperature.

Also, the catalytic reaction takes place only when oxygen and water are co-added to NO in the gas flow, as shown in Figure 3. The presence of NO alone doesn't promote any catalytic reaction (Fig. 3a, S1). The addition of oxygen provokes a consistent oxidation of NO to NO_2 (about 45%, Fig. 3a, S2), whereas only the successive introduction of water in the gas flow promotes the catalytic activity for NOx elimination (Fig. 3b, S3).

Considering now the concomitant IR spectra of the material, we observe that sending a flow containing 1000 ppm NO, 10% O_2, 1% H_2O in Ar as the vector gas on the sample at about 300 K provokes, first, the formation of NO adsorbed species on iron sites, as witnessed by the doublet at 1841 and 1827 cm^{-1}, typical for nitrosyls on Fe^{II} [19] (Figure 2b).

After time on stream, while the nitrosyls decrease other bands appear in the region 2300-1600 cm^{-1}. The band at 1879 cm^{-1} can be associated with the $\nu(N=O)$ stretches of adsorbed N_2O_3 species, being the $\nu_{as}(NO)_2$ mode hidden by the carboxylate massif and the $\nu_s(NO)_2$ mode contained in the small massif centered at 1285 cm^{-1} (Extended Data Figure 6)[55]. The band at 1773 cm^{-1} can be assigned to the $\nu(-O=N)$ vibration of the antisymmetric NONO, which is produced at a low temperature in the presence of Lewis acid sites**Erreur ! Signet non défini.**. The alternative to assign the features at 1879 and 1773 cm^{-1} to dinitrosyls, probably bent[55], would be inaccurate: (i) if the 1879 and 1773 cm^{-1} bands are assigned to the same species, they should have the same kinetics, which is not the case (see Figure 2b & c); (ii) it is quite unlikely that dinitrosyls appear when the consumption of mononitrosyls by reaction becomes evident. The bands at 1715 and 1733 cm^{-1} are likely due to adsorbed NO_2 or N_2O_4 (presenting also a band at 2185 cm^{-1}). Since NO and O_2 were fed in the gas mixture, we can conclude that oxidation of NO into NO_2 has taken place on the surface as confirmed by the analysis of the exhaust gas in Fig. 2d and 3. The described evidence is not an obvious result. In fact, some of metal oxides (such as Mn and Ce-based oxides[56]) are known to catalyze the oxidation reaction of NO into NO_2. However, this phenomenon has never been observed on a MOF, or on iron oxide to the best of our knowledge, but only on iron porphyrins[57]. Additionally, the oxidation is also effective in the presence of only Fe^{III} sites in MIL-100(Fe), as observed in Extended Data Fig. 1.

Considering the additional bands present at lower wavenumbers (Fig. 2b and Extended Data Fig. 6), we can tentatively assign the doublets at 1696-1683 and 1133-1123 cm^{-1} to nitrates, while the bands at 1285 and 1238 cm^{-1} are compatible with the presence of nitrites[55,58], even if the intense modes of carboxylates impeach band resolution in this region of the spectra. Interestingly, when these nitrogen-containing species are formed NO^+ moieties are concomitantly detected, as indicated by a band at 2188 cm^{-1} (Extended Data Fig. 7), similar to that formed on zeolites in similar conditions and considered as an intermediate for NOx

reduction[Erreur ! Signet non défini.]. In the present case we cannot decide yet if these species are relevant for the reaction mechanism or if they are barely spectators.

Scrutinizing the spectra in the Extended Data Figure 7, we also remark that nitrosyls on Fe^{3+} appear since the first contacts between the surface and the gas phase (bottom spectra), giving rise to a band at 1901 cm^{-1}, much weaker than the corresponding species on Fe^{2+}, as already remarked[22,34]. This band follows the trend of those for the other nitrosyls, i.e. increasing, then decreasing, until to be undetectable, due to the overlapping with the overtones of structural bands in the 1950-1870 cm^{-1} region, perturbed by the formation of adsorbed phases. Similarly, the features of bands between 2150 and 1950 cm^{-1} are difficult to interpret; looking at the direct spectra (Extended Data Figure 8), they seem to be due to changes in the background spectra, enhanced by the difference between each spectrum and the reference. We can mention that Busca and Lorenzelli reported the presence of NO_2^- in this region[59], which is not unlikely.

In the OH stretching region we observe the formation of sharp bands at 3680 and 3604 cm^{-1} assigned to molecular water coordinatively adsorbed on Fe^{3+} CUS, and a broad massif around 3100 cm^{-1} due to H-bonded water species[22]. The pristine Fe^{II} hydroxyls[60] at ~3621 cm^{-1} progressively disappear during the chemical reaction, in parallel with nitrosyls on Fe^{2+}. Additional bands are formed at 3700 and 3674 cm^{-1}. Are these features related with the NO reduction mechanism? It is likely the case, considering that (as mentioned above) the presence of water is necessary to observe the catalytic reaction although their role is still unclear.

To better understand the phenomena taking place on the surface of MIL-100(Fe) and correlate them with the species observed in the gas phase, it is worth considering the kinetic behaviour of each entity. Fig. 2c shows the intensity profiles of the aforementioned species versus reaction time at the initial stage of the reaction. The time sequence for N-containing species appearing and disappearing is quite clear. Nitrosyl species are first formed on Fe^{II} sites, until their intensities reach a maximum, and then decrease. NO_2 is also formed first on the surface of the sample, and then detected in the gas phase. The proximity between coordinated NO and NO_2 gives rise to N_2O_3 moieties, to nitrates (nitrites) and NO^+ species, while hydroxyls are perturbed and consumed (being partially restored by water in the vapour phase). This is normally proposed to happen through HNOx intermediates, which cannot be revealed here due to the vibrational modes of carboxylates superimposed to their typical bands[Erreur ! Signet non défini.]. Therefore, we can imagine that hydroxyls may have a role in the formation of these HNOx intermediates, if any.

Tentative reaction scheme for NO reduction at room temperature

Considering the spectroscopic evidences and all the elements provided in the above-mentioned discussion, we can hypothesise a global reaction mechanism, as represented in Extended Data Figure 9: (i) NO is first adsorbed on neighbouring Fe(II) and Fe(III) sites; (ii) on the latter it is oxidized to NO_2, with the concomitant reduction of the adsorption iron site; (iii) N_2O_3 is formed, but in the presence of water (coordinated or split as OH groups) it is destabilised (iv), forming nitrogen protoxide upon oxygen release. At this step (v), N_2O decomposes yielding nitrogen and reoxidising the Fe(II) site to the original Fe(III) centre; (vi) after then, the sites are finally only occupied by hydroxyls and weakly adsorbed water, so ready for a new catalytic cycle.

Obviously this description is speculative at this stage, but it is interesting to remark that the first three steps well matches with the spectroscopic evidences mentioned above, while the additional ones have already been evoked to explain the NO decomposition mechanism on Cu-zeolites, and found to be favourable at low temperature[61,62]. The oxygen release mentioned in step (iv) cannot be evidenced experimentally for technical reasons and in the absence of isotopically labelled oxygen species. However, dedicated experiments have discarded the possibility that oxygen could be adsorbed molecularly and reoxidation phenomena were not evidenced at this step. Therefore, considering that the reaction is catalytic and that the yielded nitrogen matches with the mass balance in the NO conversion, oxygen can only be released.

Additionally, two evidences plead in favour of the reaction pathway scheme described above:

i) the kinetics of the most relevant species presented in Fig. 2c presents the typical trend of a consecutive reaction: the primary reactant (NO) coordinates with the iron reaction sites, as visualised by the decreasing of the Fe-hydroxyls; iron nitrosyls are formed, they increase in intensity reaching a maximum, then decrease (as a typical intermediate) when NO_2 and N_2O_3 are formed; at this moment the final product N_2 is produced.

ii) Preliminary studies (not shown here for the sake of brevity) on similar non-redox MOFs as, for example, MIL-100(Cr)) show the above mentioned species on the surface, but N_2O is yielded in spite of nitrogen.

Additionally, to verify a fundamental part of the mechanism and the central role of nitrogen oxide into nitrogen dioxide transformation, we have repeated the reaction feeding the catalyst with a mixture of 500 ppm NO + 500 ppm NO_2, instead of 1000 ppm NO. If NO_2 is an intermediate, its direct introduction should favour the reaction, skipping the potential limiting step. Effectively, as evidenced in Extended Data Figure 10, the efficiency rises from 8% to 34% at GHSV = 15000 h^{-1}. But further studies should be performed to ascertain this and other points.

Reactivity tests on MIL-127(Fe), MIL-53(Fe) and MIL-102(Fe) samples
MIL-127(Fe), MIL-53(Fe) and MIL-102(Fe) samples were submitted to the same catalytic tests as MIL-100(Fe), using the same gas composition, contact time and powder amount. Catalytic results showed a similar NO conversion for MIL-127(Fe) as that measured for MIL-100(Fe), within the experimental error. On the opposite, at the steady state, no nitrogen monoxide conversion was measured for the other two samples.

Introduction of impurities in the reaction flow
In the experimental conditions used to assess the MIL activity for NO decomposition we have skipped carbonic impurities in the feeding flow to keep the quantification on nitrogen yield unambiguous, without contributions to m/z = 28 other than provided by N_2. Successively, the effect on the reaction of gaseous species typically present in the combustion engine exhaust has been investigated. Obviously, the survey of all the impurities present in real exhaust is outside the purpose of the present report; we have considered only the gases present in the highest concentrations and currently analysed in deNOx studies.

We didn't expect a big effect of CO or hydrocarbons on NOx adsorption, because we already found that NO adsorption on Fe^{2+} site is stronger (see results in references 19 and 22). But we have preferred to verify adding CO in the reaction flow. Even, to better simulate the

conditions offered by an automotive exhaust, we have mixed to the flow CO and H_2 in a 3:1 ratio (as it results from gasoil combustion; see for example[63]). Up to a concentration of 6.4% CO and 2.13% H_2 (well above the currently measured concentrations) we haven't found any effect on the reaction.

In respect to sulfur compounds, MIL-100(Fe) has shown poor affinity[64].

Concerning CO_2, in a recent past we have performed deep investigations on CO_2 capture and storage in different MOF families. Among them, MIL-100 was not the most efficient material for trapping carbon dioxide [65]. Moreover, considering that the sample can be totally regenerated by CO_2 adsorption already at 303 K and that water competes with CO_2 on the adsorption sites[65], the influence of carbon dioxide on the NO adsorption and reaction cannot be relevant. However, considering the high concentrations of CO_2 in all the combustion exhausts, this point needed verification. Therefore we have repeated the experiments in the presence of carbon dioxide and verified that NO always wins the competition with CO_2 on the adsorption sites. Consequently, the reactivity was found unchanged in an appreciable way.
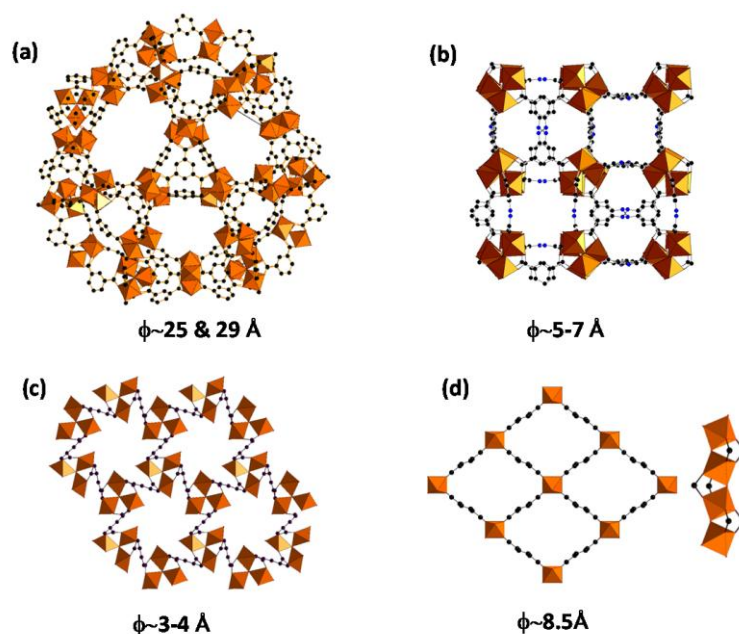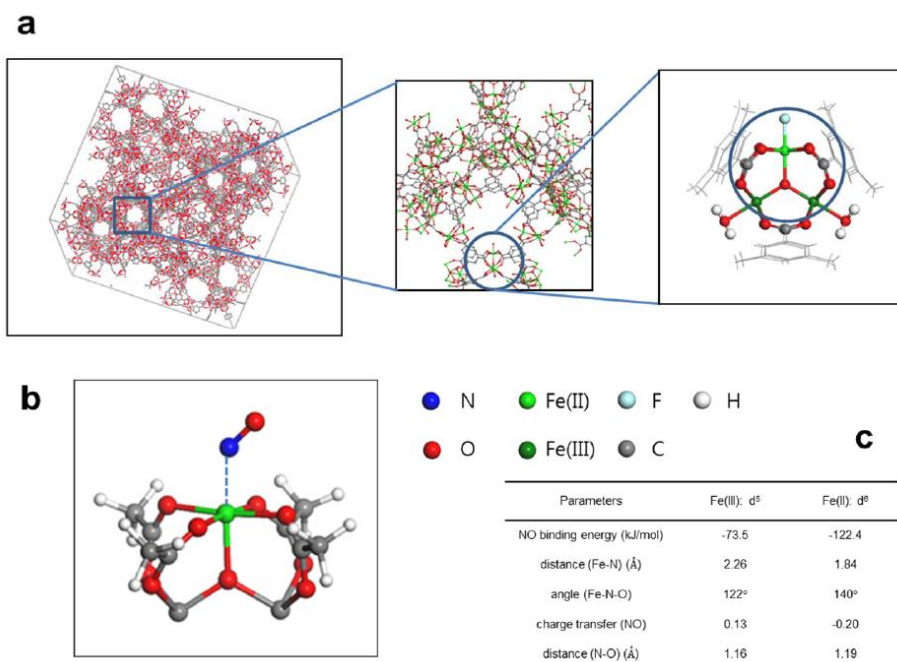
Extended Data
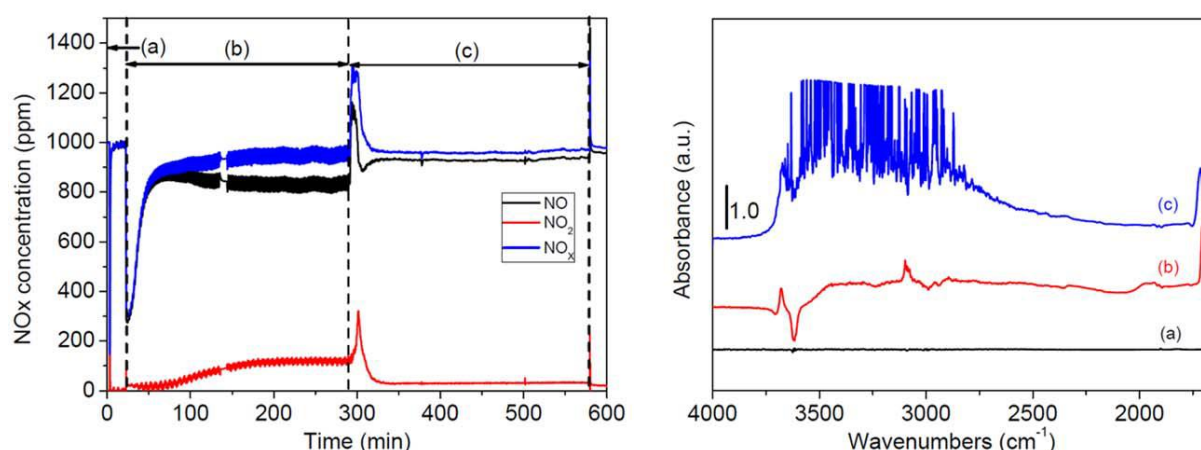
Extended Data Figure 1: effect of the activation temperature. Left: NOx concentrations (chemiluminescence profiles) after gas contact with the MIL-100(Fe) sample submitted to a flow of 1000 ppm NO (a), then adding 10% O_2 (b) and 1% H_2O (c), after activation at 423 K. Data show that no deNOx reaction is detected (but NO to NO_2 partial oxidation can be observed). Right: transmission FTIR spectra of the corresponding sample surface at the steady state, showing the absence of Fe^{II} sites on the sample surface.
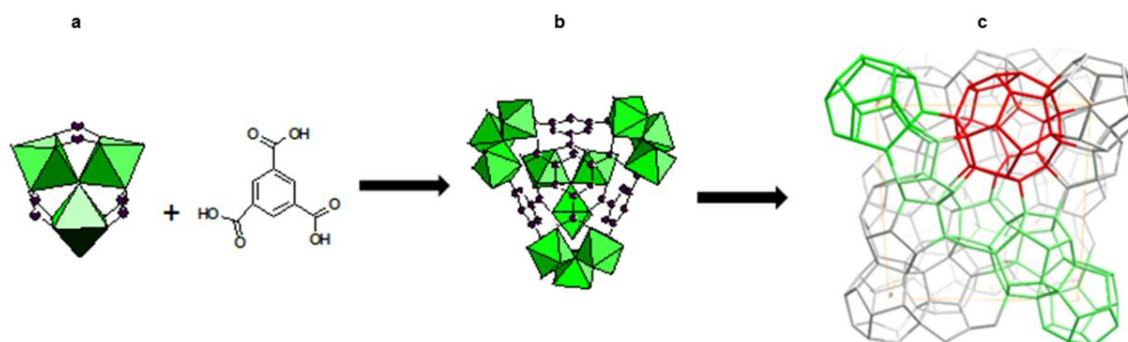
Extended Data Figure 2: Structure of MIL-100. a, the secondary building unit (trimer of chromium, octahedral) and the organic liker (1,3,5-BTC = benzene tricarboxylic or trimesic acid); b, the hybrid supertetrahedron; c, unit cell of MIL-100 with a schematic view of the MTN topology (Figure published in reference19).


Extended Data Figure 3: Schematic representation of the structure of MIL-100(Fe) (a), MIL-127(Fe) (b), MIL-102(Fe) (c) and MIL-53(Fe) (d) solids.

Extended Data Figure 4: DFT model of MIL-100(Fe). a an extended cluster model taken from the MIL-100(Fe) crystal structure. b Fe small cluster model taken from the circle in the large cluster with adsorbed NO molecule; c Table: results on cluster model DFT calculations for NO binding on reduced MIL-100(Fe).
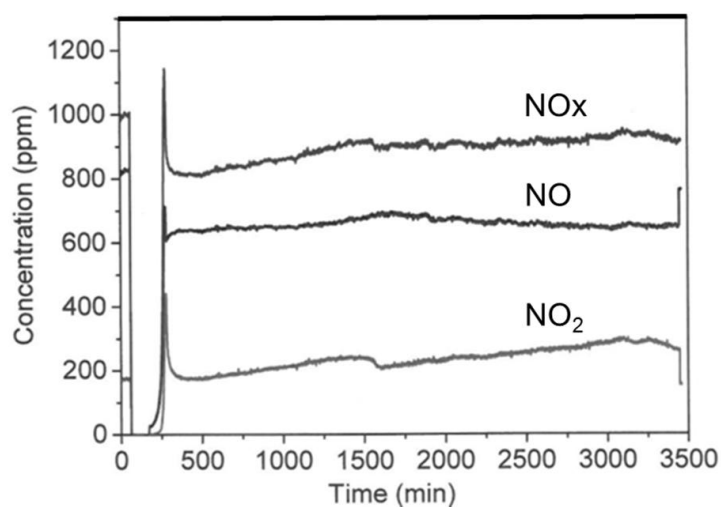

Extended Data Figure 5: NOx species profiles during a long test (> 58 hours). NOx species profiles in the gas phase after contact with partially reduced MIL-100(Fe) sample at 300 K, gas feeding with 1000 ppm NO, 10% O_2 and 1% H_2O vapour.
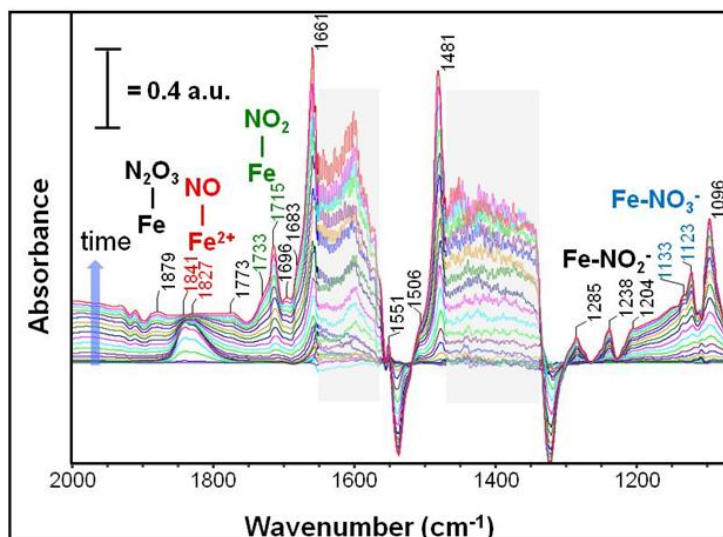
Extended Data Figure 6: IR spectral region of the sample, highlighting the presence of adsorbed N-containing species. Transmission FTIR spectra (after subtraction of the reference spectrum at t = 0) of the sample activated at 523 K, then submitted to the reaction stream; spectra are collected at given intervals of time during the reaction. The main bands affected by the gas contact with the sample are reported, pointed and labelled. They correspond both to adsorbed species vibrational modes and perturbation of the structural features (carboxylate vibrations, whose stretches are covered by the grey zones).
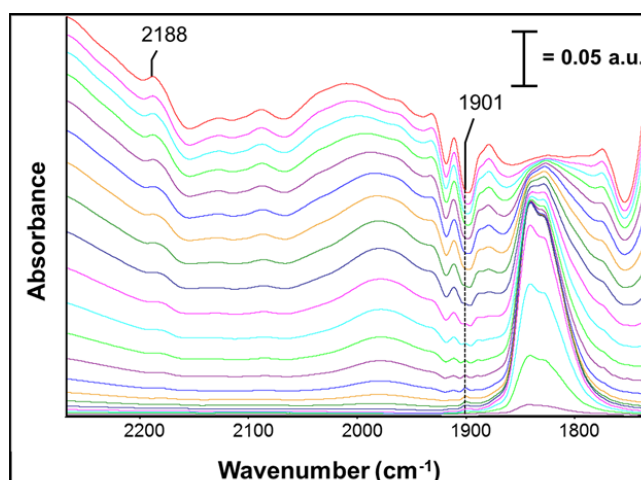

Extended Data Figure 7: highlighting the NO$^+$ vibration. Transmission FTIR spectra (after subtraction of the reference spectrum at t = 0) of the sample activated at 523 K, then submitted to the reaction stream; spectra are collected at given intervals of time during the reaction. Zoom in the region 2300-1700 cm^{-1}.
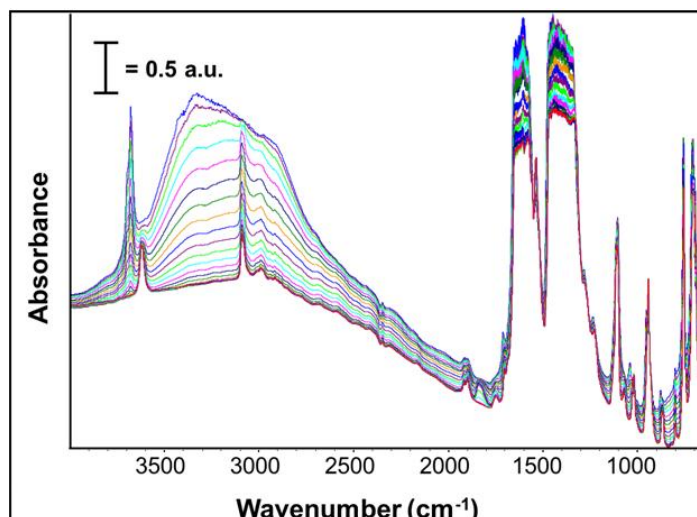
Extended Data Figure 8: Transmission FTIR direct spectra of MIL-100(Fe) in the MIDIR region. The sample was activated at 523 K, then submitted to the reaction stream; spectra are collected at given intervals of time during the reaction.
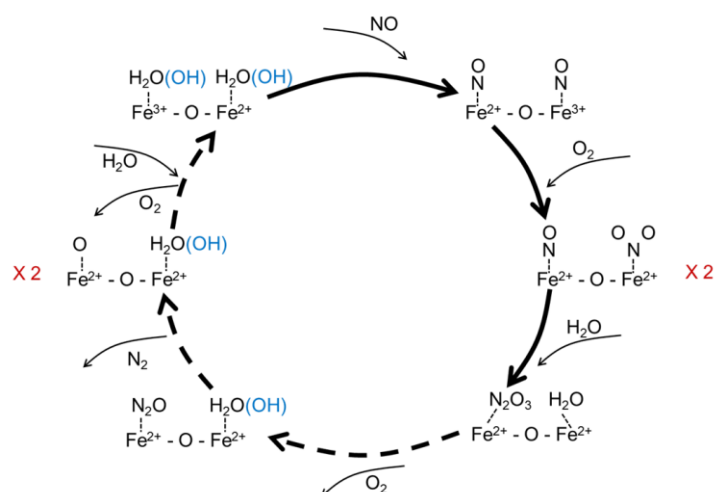
Extended Data Figure 9: Tentative reaction scheme for NO dissociation on MIL-100(Fe). Additional explanations about the scheme in more detail are made in Supplementary Information. The arrows in full line represent the (believed) main reaction steps and intermediates, as observed on the catalytic surface. The arrows in dotted line complete the catalytic reaction cycle according to models accepted in the literature (ref. 60 and 61).
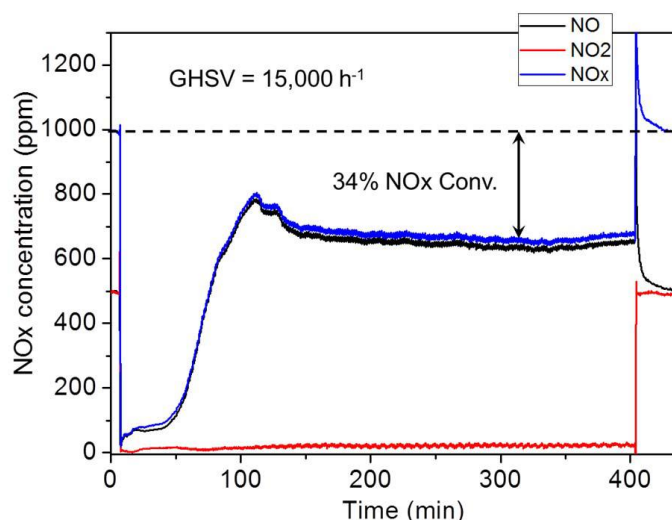
Extended Data Figure 10: effect of NO₂ introduction. NOx concentrations (chemiluminescence profiles) after gas contact with the MIL-100(Fe) sample submitted to a flow of 500 ppm NO + 500 ppm NO_2, 10% O_2 and 1% H_2O, after activation at 523 K.

Additional References

[33] Treacy, M.M.J., Higgins, J.B. in Collection of Simulated XRD Powder Patterns for Zeolites, 4th ed., Elsevier 2001, and http:// www.iza-structure.org/databases/.

[34] Vimont, A. et al. Investigation of Acid Sites in a Zeotypic Giant Pores Chromium(III) Carboxylate. *J. Am. Chem. Soc.* **128**, 3218-3227 (**2006**).

[35] Yoon, et al. Controlled Reducibility of a Metal–Organic Framework with Coordinatively Unsaturated Sites for Preferential Gas Sorption. *Angew. Chem. Int. Ed.* **49**, 5949-5952 (2010).

[36] Liu, Y., *et al*. Assembly of metal-organic frameworks (MOFs) based on indium-trimer building blocks: A porous MOF with soc topology and high hydrogen storage. *Angew. Chem. Int. Ed.* **46**, 3278-3283 (2007).

[37] O'Keeffe, M., Eddaoudi, M., Li, H.L., Reineke, T., Yaghi, O.M. Frameworks for extended solids: Geometrical design principles. *J. Solid State Chem.* **152**, 3-20 (2000).

[38] Serre, C. *et al*. Utilisation d'un solide hybride cristallin poreux comme catalyseur de réduction d'oxydes d'azote et dispositifs, 106660/FR filed 28/05/2009 ; PCT/ FR2010/000402 (28/05/2010) ; WO2010136677.

[39] Whitfield, T.R., Wang, X., Liu, L., Jacobson, A.J. Metal-organic frameworks based on iron oxide octahedral chains connected by benzenedicarboxylate dianions. *Solid Sta. Sci.* **7**, 1096-1103 (2005).

[40] Férey, G. & Serre, C. Large breathing effects in three-dimensional porous hybrid matter: facts, analyses, rules and consequences. *Chem. Soc. Rev.* **38**, , 1380-1399 (2009).

[41] Kitagawa, S. & Uemura K. Dynamic porous properties of coordination polymers inspired by hydrogen bonds. *Chem. Soc. Rev.* **34**, , 109-119 (2005).

[42] Horike, S., Shimomura, S., Kitagawa, S. Soft porous crystals. *Nature Chem.* **1**, 695-704 (2009).

[43] Millange, F., Serre, C., Guillou, N., Férey, G., Walton, R.I. Structural effects of solvents on the breathing of metal-organic frameworks: An in situ diffraction study. *Angew. Chem. Int. Ed.* **47**, 4100-4105 (2008).

[44] Delley, B. An all-electron numerical-method for solving the local density functional for polyatomic-molecules. *J. Chem. Phys.* **92**, 508-517 (1990).

[45] Delley, B. From molecules to solids with the DMol(3) approach. *J. Chem. Phys*. **113**, 7756-7764 (2000).

[46] Kresse, G. & Furthmüller, J. Efficient iterative schemes for ab initio total-energy calculations using a plane-wave basis set. *Phys. Rev. B* **54**, 11169-11186 (1996).

[47] Henkelman, G., Arnaldsson, A., Jónsson, H. A fast and robust algorithm for Bader decomposition of charge density. *Comput. Mater. Sci*. **36**, 354-360 (2006).

[48] Tkatchenko A. & Scheffler, M. Accurate Molecular Van Der Waals Interactions from Ground-State Electron Density and Free-Atom Reference Data. *Phys. Rev. Lett*. **102**, n° 073005 (2009).

[49] Kresse, G. & Joubert, D. From ultrasoft pseudopotentials to the projector augmented-wave method. *Phys. Rev. B* **59**, 1758-1775 (1999).

[50] Grimme, S. Semiempirical GGA-type density functional constructed with a long-range dispersion correction. *J. Comp. Chem*. **27**, 1787-1799 (2006).

[51] Lesage, T., Verrier, C., Bazin, P., Saussey, J., Daturi, M. Studying the NOx-trap mechanism over a Pt-Rh/Ba/Al_2O_3 catalyst by *operando* FT-IR spectroscopy. *Phys. Chem. Chem. Phys*. **5**, 4435-4440 (2003).

[52] Malpartida, I. *et al.* CO and NO adsorption for the IR characterization of Fe^{2+} cations in ferrierite: An efficient catalyst for NOx SCR with NH_3 as studied by *operando* IR spectroscopy. *Catal. Today* **149**, 295-303 (2010).

[53] Rasmussen, S.B., Perez-Ferreras, S., Bañares, M.A., Bazin, P., Daturi, M. Does Pelletizing Catalysts Influence the Efficiency Number of Activity Measurements? Spectrochemical Engineering Considerations for an Accurate Operando Study. *ACS Catal*. **3**, , , 86-94 (2013).

[54] Rasmussen, S.B., Perez-Ferreras, S., Bañares, M.A., Bazin, P., Daturi M. Does Pelletizing Catalysts Influence the Efficiency Number of Activity Measurements? Spectrochemical Engineering Considerations for an Accurate Operando Study. *ACS Catal*. **3**, 86-94 (2013).

[55] Hadjiivanov, K.I. Identification of Neutral and Charged N_xO_y Surface Species by IR Spectroscopy. *Catal. Rev.—Sci. Eng*. **42**, 71-144 (2000).

[56] Lesage, T. *et al.* Operando FTIR study of NOx storage over a Pt/K/Mn/Al_2O_3-CeO_2 catalyst. *Appl. Catal. B: Environmental* **72**, 166-177 (2007).

[57] Lei, J.P., Ju, H.X., Ikeda, O. Catalytic oxidation of nitric oxide and nitrite mediated by water-soluble high-valent iron porphyrins at an ITO electrode, *J. Electroanalytical Chemistry* **567**, 331-338 (2004).

[58] Chen, H.-Y., El-Malki, E.M., Wang, X., van Santen, R.A., Sachtler, W.M.H. Identification of active sites and adsorption complexes in Fe/MFI catalysts for NOx reduction. *J. Mol. Catal. A: Chem.* **162**, 159-174 (2000).

[59] Busca, G., Lorenzelli, V. Infrared study of the adsorption of nitrogen-dioxide, nitric-oxide and nitrous-oxide on hematite. *J. Catal.* **72**, 303-313 (1981).

[60] Rémazeilles, C., Refait, Ph. Fe(II) hydroxycarbonate Fe-2(OH)(2)CO_3 (chukanovite) as iron corrosion product: Synthesis and study by Fourier Transform Infrared Spectroscopy. *Polyhedron* **28**, 749-756 (2009).

[61] Solans-Monfort, X., Branchadell, V., Sodupe, M. On the NO Decomposition by Cu-ZSM-5 through the ZCu(NO_2)(NO) or ZCu(N_2O_3) Intermediates. *J. Phys. Chem. B* **106**, 1372-1379 (2002).

[62] Aylor, A.W., Larsen, S.C., Reimer, J.A. Bell, A.T. An infrared study of NO decomposition over Cu-ZSM-5. *J. Catal.* **157**, 592-602 (1995).

[63] Dupré, J. et al. Understanding the storage function of a commercial NOx-storage-reduction material using operando IR under realistic conditions. *Appl. Catal. B: Environ.* **160**, 335-343 (2014).

[64] Van de Voorde, B. et al. N/S-heterocyclic contaminant removal from fuels by the mesoporous metal-organic framework MIL-100: the role of the metal ion. *J. Am. Chem. Soc.* **135**, 9849−9856 (2013).

[65] Llewellyn, P. et al. High uptakes of CO_2 and CH_4 in the mesoporous Metal-Organic-Frameworks MIL100 and MIL101. *Langmuir* **24**, 7245-7250 (2008).